Interface Study of the Intermediate Connectors in Tandem Organic Devices

Jian-Xin Tang[a], Man-Keung Fung[b], Chun-Sing Lee[b], and Shuit-Tong Lee[b]

Abstract

The intermediate connectors play crucial roles in the performance of tandem organic light-emitting diodes (OLEDs) because they are required to facilitate charge carrier transport and to guarantee transparency for light transmission and deposition compatibility. Understanding the physical properties of the intermediate connector is not only fundamentally important but is also crucial to developing high-efficiency organic devices with a tandem structure. In this study, several effective intermediate connectors in tandem OLEDs using a doped or non-doped organic p-n heterojunction were systematically investigated by studying their interfacial electronic structures and corresponding device characteristics. The working mechanisms of the intermediate connectors are discussed herein by referring to their relevant energy levels with respect to those of the neighboring organic layers. The factors affecting the operation of the intermediate connectors in tandem OLEDs, as demonstrated herein, provide guidance for the identification of new materials and device architectures for high-performance devices.

Keywords: tandem OLED, stacked structure, intermediate connector, *p-n* heterojunction, doping

1. Introduction

Organic light-emitting diodes (OLEDs) have been inducing widespread research and drawing commercial interest for their applications in next-generation flat panel displays and solid-state lighting [1-5]. As a current-driven device, an OLED must be operated at a relatively high current density to achieve high brightness. The life of an OLED decreases, however, with increased driving current density. To increase both the luminous efficiency and the life of OLEDs, a tandem (or stacked) structure has been proposed, where all of the individual electroluminescent (EL) units are electrically connected in series by inserting an intermediate connector between the adjacent EL units [6-15]. Thus, in principle, the EL intensity, current efficiency, and life of tandem OLEDs can linearly increase with the number of EL units (as shown in Fig. 1). In addition, the tandem structure makes it possible for EL units of different colors to be vertically stacked for tuning the device color and enhancing the device performance [11-15].

The intermediate connector plays a crucial role in the performance of tandem OLEDs, whose intermediate connectors should facilitate effective electron injection and hole blocking into one of the connected EL units while performing the opposite role for the other connected emitting unit. The intermediate connectors must also be highly transparent for light transmission, must maintain low series

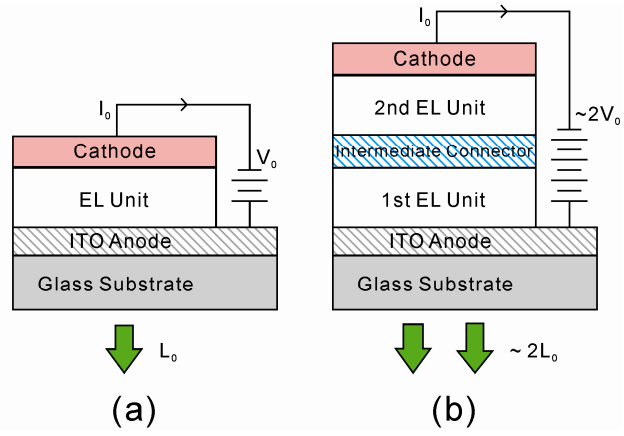

Fig. 1. Schematic structures of (a) a conventional OLED with a single EL unit, and (b) a tandem OLED with two identical EL units.

Manuscript Received November 16, 2009; Revised February 16, 2010; Accepted for publication February 24, 2010
These authors wish to thank the City University of Hong Kong, SRG (Grant No. 7002434), China's National High-Tech R&D Program (863 Program; No. 2008AA03A327), and the National Natural Science Foundation of China (No. 60937001) for the financial support they provided for this research work.
Corresponding author : Jian-Xin Tang
[a] Functional Nano & Soft Materials Laboratory (FUNSOM) & Jiangsu Key Laboratory for Carbon-based Functional Materials and Devices, Soochow University, Suzhou 215123, China
[b] Center of Superdiamond and Advanced Films (COSDAF) and Department of Physics and Materials Science, City University of Hong Kong, Hong Kong SAR, China
E-mail: jxtang@suda.edu.cn **Tel:** +86-512-6588-0942 **Fax:** +86-512-6588-2846

resistance for minimal electrical loss, and must guarantee deposition compatibility and stability. Extensive efforts have been devoted to the exploration of high-performance intermediate connectors, which typically consist of a *p*-*n* junction. The *p*-type layer of the intermediate connector is usually formed by metal oxides, including indium-tin-oxide (ITO) [16, 17], V_2O_5 [6], WO_3 [11, 12], MoO_3 [7, 13, 14], or an organic hole-transporting layer (HTL) doped with Lewis acid (e.g., $FeCl_3$:NPB) [8], while the *n*-type layer is usually prepared by doping an electron-transporting layer (ETL) with low-work-function metals, such as Cs [6, 16, 18], Li [6, 8, 13, 14], and Mg [11, 12, 19-22].

The use of metal oxides in the intermediate connectors, however, usually causes fabrication incompatibility due to the high thermal-evaporation temperature or low optical transparency. It is therefore desirable to explore the feasibility of replacing metal oxides with more compatible organic systems as the intermediate connectors because such systems can be deposited with relatively low evaporation temperatures and high optical transparency. In addition, the working mechanism of an intermediate connector in a tandem OLED is not yet well understood. In particular, electronic structures, including various relevant electron energy levels at the interfaces of the intermediate connectors, are still unavailable. It is necessary to provide systematic information on how the performance of an intermediate connector is related to its constituent materials.

In this work, a systematic investigation of tandem OLEDs was carried out, and several effective organic *p*-*n* heterostructured intermediate connectors for tandem OLEDs were demonstrated using a doped or non-doped organic *p*-*n* heterojunction [20-23]. Through a combination of interface study and device fabrication, the influence of the *n*- or *p*-type organic layer in intermediate connectors on device performance was investigated, and physical insights were provided for exploring new structures for an effective intermediate connector with a reduced drive voltage, improved voltage stability, and improved power efficiency for tandem OLEDs.

2. Experiments

Tandem OLEDs were fabricated onto a patterned ITO-coated glass substrate (30 Ω/sq) with two individual EL units, each consisting of an HTL and an ETL. The EL units were separated by intermediate connectors with varied organic heterostructures. For comparison, standard devices with a single EL unit were also prepared. Prior to film deposition, the ITO substrates were cleaned with Decon 90, rinsed in de-ionized water, dried in an oven, and finally treated in an ultraviolet (UV) ozone cleaner. The organic and metal layers were thermally evaporated at a base pressure of 5×10^{-6} Torr. The deposition rates of the different layers were monitored with a quartz oscillating crystal and were maintained at 1–2 Å/s for both the organics and the metals, while the dopant and host materials were co-evaporated with a rate ratio of 0.2:1 Å/s. A shadow mask was used to define the cathode and to fabricate four 0.1-cm^2 devices on each substrate. The detailed layer structures of the OLEDs that were fabricated in this work are shown in Table 1.

The current density-voltage-luminance (J–V–L) characteristics and electroluminescence spectra were measured simultaneously with a programmable Keithley model 237 power source and a Photoresearch PR 650 spectrometer. The interface study was carried out in a VG ESCALAB 220i-XL photoelectron spectroscopy system, which consists of an analysis chamber interconnected to an evaporation chamber. The base pressures in the evaporation and analysis

Table 1. OLED layer structures

Device/ Unit	Layer Structures
A	ITO/**EL1**/Mg:Alq_3(10nm, 10vol%)/m-MTDATA (20nm) /**EL1**/Mg:Ag(200nm)
B	ITO/**EL1**/Alq_3(10nm)/F_4-TCNQ:m-MTDATA(20nm, 5vol%)/ EL1/Mg:Ag(200nm)
C	ITO/**EL1**/Mg:Alq_3(10nm, 10vol%)/F_4-TCNQ:m-MTDAT A(20nm, 5vol%)/**EL1**/Mg:Ag(200nm)
D	ITO/EL1/Mg:Ag(200nm)
EL1	NPB(60nm)/Alq_3(40nm)
E	ITO/**EL2**/Mg:Alq_3(10nm, 20vol%)/WO_3(4nm)/**EL3**/Ca (15nm)/Ag(100nm)
F	ITO/**EL2**/Yb:Alq_3(10nm, 20vol%)/WO_3(4nm)/**EL3**/Ca (15nm)/Ag(100nm)
G	ITO/**EL2**/Ca:Alq_3(10nm, 20vol%)/WO_3(4nm)/**EL3**/Ca (15nm)/Ag(100nm)
H	ITO/**EL2**/Mg:PyPySPyPy(10nm, 20vol%)/WO_3(4nm)/**E L3**/Ca(15nm)/Ag(100nm)
I	ITO/**EL2**/Mg:BPhen(10nm, 20vol%)/WO_3(4nm)/**EL3**/Ca (15nm)/Ag(100nm)
J	ITO/**EL2**/Mg:CuPc(10nm, 20vol%)/WO_3(4nm)/**EL3**/Ca (15nm)/Ag(100nm)
K	ITO/**EL3**/Ca(15nm)/Ag(100nm)
EL2	NPB(70nm)/Alq_3(40nm)
EL3	NPB(70nm)/Alq_3(50nm)
L	ITO/**EL4**/Yb(15nm)/Ag(100nm)
M	ITO/**EL4**/F_{16}CuPc(5nm)/CuPc(5nm)/**EL4**/Yb(15nm)/Ag (100nm)
EL4	NPB(70nm)/MADN(40nm)/BPhen(10nm)

chambers were 8×10^{-10} and 5×10^{-10} Torr, respectively. The ITO substrate was *ex-situ* treated with UV ozone exposure, and the organic materials were *in-situ* evaporated in steps onto the substrates in the preparation chambers, with a growth rate of 1-2 Å/s. The samples were transferred to the analysis chamber without a vacuum break for the measurements after each deposition step. The ultraviolet photoelectron spectrum (UPS) measurements were performed using an unfiltered He I (21.2 eV) gas discharge lamp, with the sample biased at -4 V. The resolution of the UPS measurements was 0.09 eV. All the measurements were carried out at room temperature.

3. Results and Discussion

3.1 Doped Organic p-n Heterostructure as the Intermediate Connector

A bilayer intermediate connector of Mg-doped tris(8-hydrooxyquinoline) aluminum(III) (Mg:Alq_3) and tetrafluoro-tetracyanoquinodimethane-doped 4,4',4"-tris{N,-(3-methylphenyl)-N-phenylamino}-triphenylamine (F_4-TCNQ:m-MTDATA) was investigated for application in tandem OLEDs, which have two identical EL units of NPB (60 nm)/Alq_3 (40 nm) connected by an intermediate connector, as shown in Table 1 (NPB: N,N'-bis(1-naphthyl)-N,N'-diphenyl-1,1'-biphenyl-4,4'-diamine). Three sets of organic bilayer intermediate connectors were used for the fabrication of tandem OLEDs (devices A-C), including (1) Mg:Alq_3/m-MTDATA, (2) Alq_3/F_4-TCNQ:m-MTDATA, and (3) Mg:Alq_3/F_4-TCNQ:m-MTDATA.

The J-V-L characteristics and luminous efficiency of the three tandem OLEDs (devices A-C, as listed in Table 1) are plotted in Fig. 2, together with those of a standard OLED with only one EL unit (device D), for comparison. As shown in Fig. 2a, the current densities of the tandem OLEDs utilizing F_4-TCNQ:m-MTDATA as the hole injection contact (devices B and C) were two orders of magnitude higher than that of the tandem OLED that did not utilize F_4-TCNQ (device A), demonstrating the significance of the F_4-TCNQ dopant in the electrical property of the organic *p-n* intermediate connector.

Fig. 2b and 2c plot the luminance and luminous efficiency as a function of the current density for the tandem and standard OLEDs. At a current density of 50 mA/cm^2, the tandem devices A, B, and C achieved about 2400, 2250, and 4200 cd/m^2 luminance and 4.8, 4.5, and 8.4 cd/A current efficiency, respectively, compared with 1800 cd/m^2 and 3.6 cd/A for the single EL device (device D). It is evident that although the driving voltage of device A (with an Mg:Alq_3/m-MTDATA intermediate connector) is about twice that of device B (with an Alq_3/F_4-TCNQ:m-MTDATA

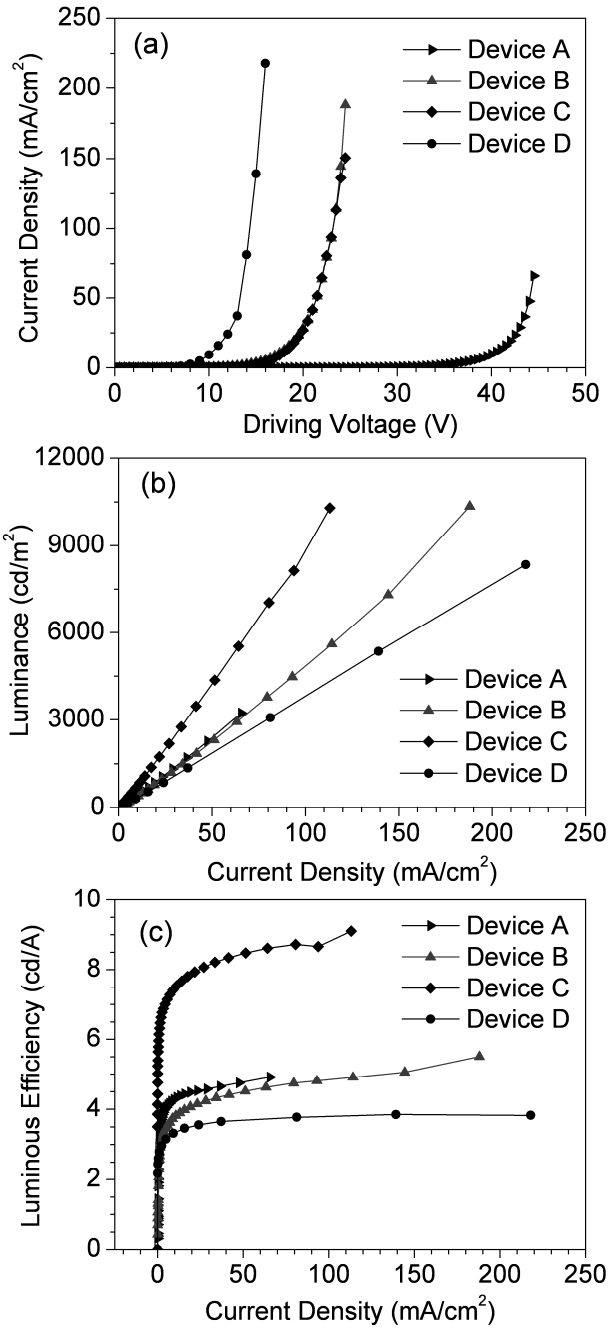

Fig. 2. (a) Current density as a function of the driving voltage, and (b) luminance and (c) luminous efficiency vs. current density for devices A–D.

intermediate connector), they have similar luminance at any current density. On the contrary, the intermediate connector of device C led to a tandem OLED with a luminous efficiency twice that of a single-unit OLED, indicating the high effectiveness of the intermediate connector used in device C. As the EL units in devices A, B, and C are identical, the discrepancy in their luminance and efficiency indicates that the intermediate connectors play a crucial role in determining the device performance of tandem OLEDs.

To understand the difference in luminous efficiency and the underlying mechanism of how these intermediate connectors work, the interface of *n*- and *p*-doped organic layers and their interfaces with the neighboring organic layers were studied via UPS measurements. Relevant data from previous UPS studies were summarized into the energy level diagrams in Fig. 3 for various intermediate connectors on UV-treated ITO substrates. The Fermi level (E_F) of the underlying ITO substrate was used as reference. The highest occupied molecular orbital (HOMO) of all the materials was obtained from the UPS measurements, and the lowest unoccupied molecular orbital (LUMO) positions of the Alq_3 layer was estimated based on the difference in the charge-transport gap (~3.7 eV) and HOMO energy level [24]. (The LUMO levels of NPB and m-MTDATA are shown here only for reference purposes.) In addition, the doped films are assumed to have the same energy gap as the pristine films. The hole (or electron) injection barriers were measured as the difference between the offset of E_F and HOMO (or LUMO).

As shown in Fig. 3, the UPS measurements show that the differences in device performance can be explained by the electronic structures of the intermediate connectors and by the interface formation between the intermediate connectors and the neighboring EL units. It was demonstrated that the presence of both Mg and F_4-TCNQ dopants provides better energy level matching, leading to the formation

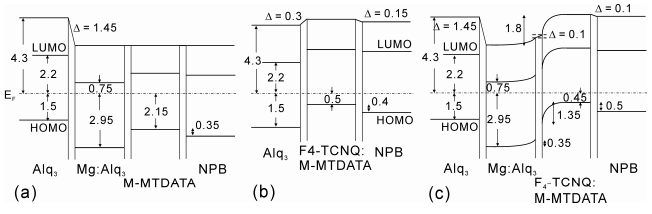

Fig. 3. Energy band diagrams for the (a) Alq_3/Mg:Alq_3/m-MTDATA/NPB, (b) Alq_3/F_4-TCNQ:m-MTDATA/NPB, and (c) Alq_3/Mg:Alq_3/F_4-TCNQ:m-MTDATA/NPB interfaces on the UV-treated ITO substrates.

of a bipolar heterojunction and thus effective charge spouting. Moreover, the insertion of Mg:Alq_3 between Alq_3 and F_4-TCNQ:m-MTDATA helps block the holes simultaneously flowing from the ITO side into the second EL unit and hence eliminates the leakage current. As a result, such intermediate connector facilitates efficient carrier injection from the intermediate connector into the carrier-transporting layers [20, 21].

3.2 Influence of the n-Type Organic Layer on the Intermediate Connector

While the characteristics of tandem OLEDs that use different intermediate connectors have been reported, the performance of the intermediate connectors cannot be directly compared due to the differences in their individual device configurations and preparation processes. In this work, the influence of the *n*-type organic layer in an intermediate connector on the performance of tandem OLEDs was investigated [22].

The tandem OLEDs were fabricated with two EL units separated by an intermediate connector with a metal-doped ETL/WO_3 structure. The *n*-type layer in an intermediate connector was modified by using either different metal dopants (e.g., Yb, Ca, and Mg) into Alq_3 (devices E-G in Table 1) or by doping Mg into four different ETL materials (e.g., Alq_3, BPhen, PyPySPyPy, and CuPc) (devices H-J in Table 1) while keeping the *p*-type layer of WO_3 unchanged (BPhen, PyPySPyPy, and CuPc denote bathophenanthroline, 2,5-bis(2',2"-bipyridin-6-yl)-1,1-dimethyl-3,4-diphenyl silacyclopentadiene, and copper phthalocyanine, respectively).

First, the correlation between the metal dopants in the intermediate connectors and the device performance was focused on. Fig. 4 shows the current J–V characteristics and current efficiency for the devices with different metal dopants in the intermediate connectors. All the tandem OLEDs showed a doubled current efficiency but required a higher driving voltage compared to the standard device (device K) to achieve the same current density.

Contrary to common belief, the device characteristics were found to be inconsistent with the work function variation of the metal dopants used here, as supported by the UPS results of the electronic structures of the metal-doped Alq_3 layers, that the LUMO of all the metal-doped *n*-type layers studied here have similar energy level alignments (see the energy level diagrams in Fig. 5) [20-22]. It can be

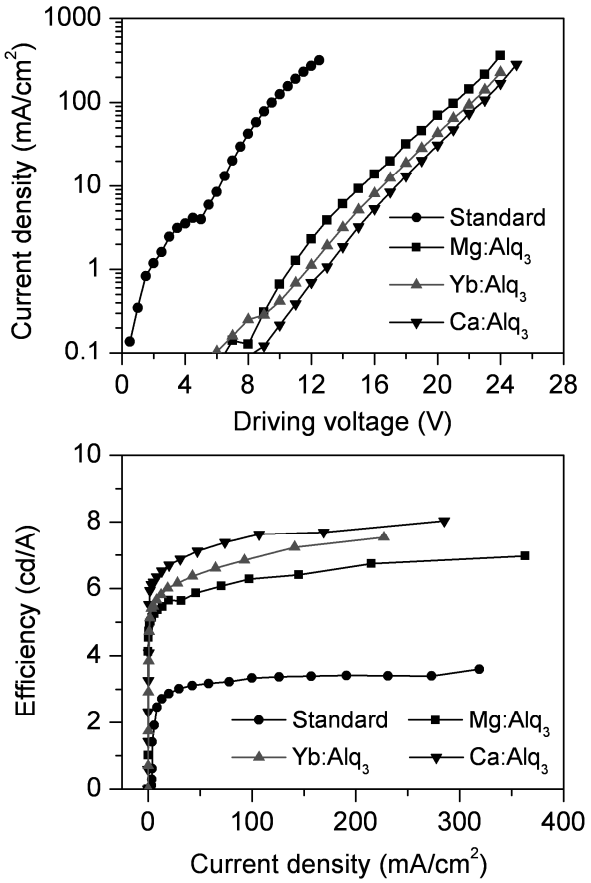

Fig. 4. (a) Current density as a function of the driving voltage. (b) Luminous efficiency vs. current density for the tandem OLEDs with different metal dopants in the intermediate connectors.

seen that metal doping in the organic layer results in sizeable band bending, clearly indicating the efficient *n*-type doping through electron transfer from the metal to the Alq_3 molecules [25]. Although the electron injection barriers

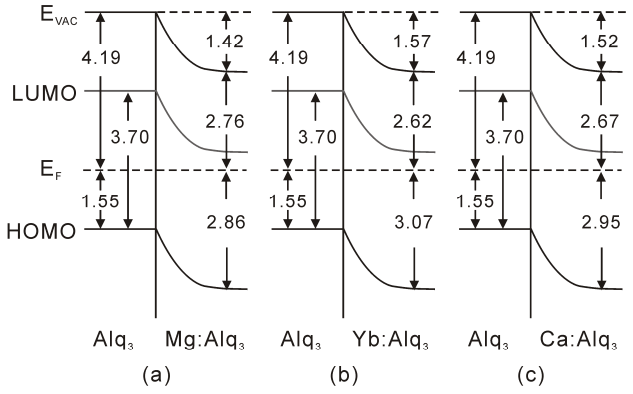

Fig. 5. Energy level diagrams for the (a) Alq_3/Mg:Alq_3, (b) Alq_3/Yb:Alq_3, and (c) Alq_3/Ca:Alq_3 interfaces.

from the intermediate connectors were found not to be sensitive to the metal dopant that was used, a strong correlation was observed between the device performance and the electrical conductivity of the metal-doped thin films. This indicates that the dominant mechanism responsible for the variation in the electrical characteristics of the tandem OLEDs shown in Fig. 4 is presumably associated with the different conductivities of the reactive metal-doped Alq_3 films in the intermediate connectors.

Apart from metal doping, the effects of the use of different ETLs in the intermediate connector were also investigated. Here, BPhen, PyPySPyPy, and CuPc were selected because of their high electron mobilities (1.2×10^{-6} [26], 1.8×10^{-6} [27], 5.2×10^{-4} [20], and 2.1×10^{-3} cm^2/V S [28], respectively, for Alq_3, PyPySPyPy, BPhen, and CuPc, at an electric field of $5.5\text{x}10^5$ V/cm). Fig. 6 plots the electrical characteristics and current efficiency of the devices with

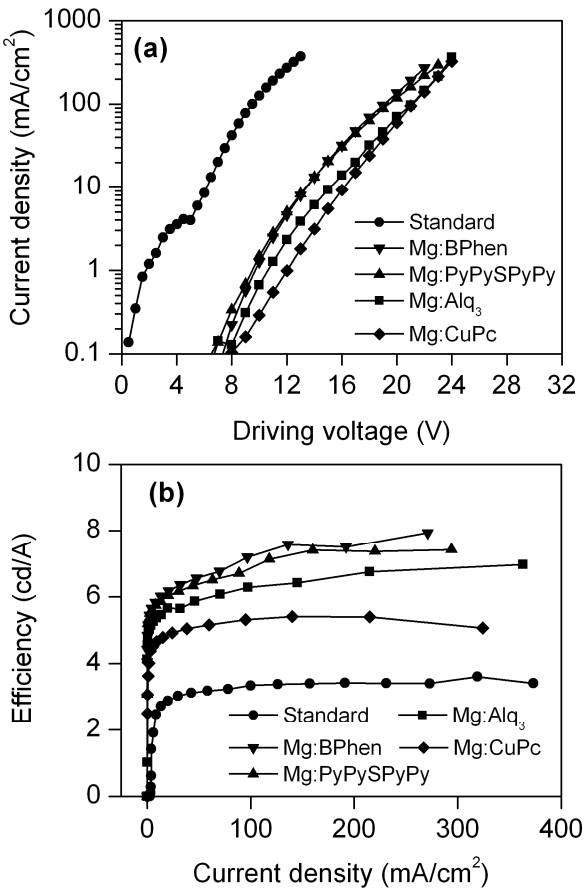

Fig. 6. Characteristics of the tandem OLEDs with different Mg:ETL/WO_3 intermediate connectors: (a) J-V characteristics and (b) current efficiency vs. current density. ETL consists of Alq_3, PyPySPyPy, BPhen, and CuPc.

different Mg:ETL/WO_3 intermediate connectors. As expected, the device utilizing an ETL with higher electron mobility showed a lower driving voltage, except for CuPc. The low electrical properties of the device with an Mg:CuPc intermediate connector are presumably due to a large electron-injection barrier at the Alq_3/CuPc interface and to the connector's relatively low optical transmittance compared to those of all the other Mg:ETL films. These results clearly indicate the importance of the high optical transparency of the intermediate connectors, which serves a guideline for selecting the *n*-type layer of the intermediate connector to improve the performance of tandem devices.

3.3 Non-doped Organic p-n Heterostructure as the Intermediate Connector

It is well known that the incorporation of diffused dopants can significantly alter the electrical conductivity of organic layers and can thus readily cause undesirable effects in the device characteristics under continuous operation. It is thus useful to replace the doped organic layer in the organic-heterojunction intermediate connector with a non-doped organic layer to be able to come up with tandem OLEDs with improved voltage stability, as well as to simplify the fabrication process. The feasibility of replacing the doped organic layers with a fully non-doped organic system of copper hexadecafluorophthalocyanine (F_{16}CuPc)/CuPc as an intermediate connector for deep-blue electrofluorescent tandem OLEDs has been explored by taking advantage of the system's ambipolar characteristics, as reported in the ambipolar field effect transistor [23, 29, 30]. Fig. 7 plots the luminance of the conventional and tandem OLEDs, where 2-methyl-9,10-di (2-naphthyl) anthracene (MADN) was used as the blue-emitting layer, as a function of the current density. Clearly, at the same current density, the tandem device (device M) exhibits luminance doubling. For instance, at a luminance of 100 cd/m^2 (the typical brightness for display application), the current density required is only 6.2 mA/cm^2 for the tandem OLED, much lower than that required for the standard device with a single EL unit (17.1 mA/cm^2). In addition, the pure organic intermediate connector showed superior optical transparency (~100%) for blue emission (around 440 nm) as well as a minimal microcavity effect in the tandem devices. These values clearly demonstrate the effectiveness of the tandem architecture with two EL units in improving the device performance.

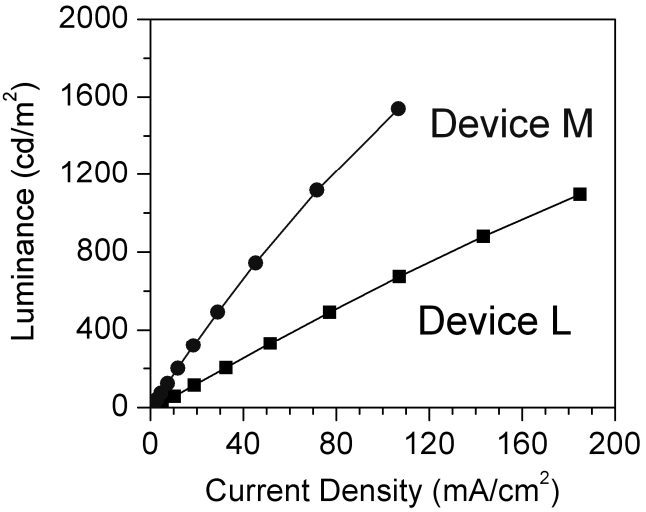

Fig. 7. Luminance as a function of the current density of the standard (device L) and tandem OLEDs (device M).

4. Summary

Several effective intermediate connectors in tandem OLEDs were investigated in this study, using a doped or non-doped organic *p-n* heterostructure to replace metal oxides and to produce high-efficiency devices. The electronic structures of the various intermediate connectors, including the relevant energy level alignment, were studied via UPS measurements to discuss their working mechanisms. It was revealed that the *p*-type doped organic films with F_4-TCNQ can be used to replace metal oxides as the *p*-type layers in the intermediate connectors. By systematically varying the metal dopants for the *n*-type organic layers in the intermediate connectors, the important factors affecting the performance of tandem OLEDs, which is dependent on the electrical conductivities of the constituent organic layers, were identified. Furthermore, a non-doped organic heterostructure made of F_{16}CuPc/CuPc was utilized as an intermediate connector in a deep-blue electrofluorescent MADN-emitting OLED. The understanding of the intermediate connectors in tandem OLEDs, as demonstrated herein, can provide guidance for the identification of new materials and device architectures for high-performance devices.

References

[1] C. W. Tang and S. A. VanSlyke, *Appl. Phys. Lett.* **51**, 913 (1987).

[2] L. S. Hung and C. H. Chen, *Mater. Sci. Eng. R* **39**, 143 (2002).
[3] B. W. D'Andrade and S. R. Forrest, *Adv. Mater.* **16**, 1585 (2004).
[4] Y. Gao, I. D. Parker, G. Yu, C. Zhang, and A. J. Heeger, *Nature* **397**, 414 (1999).
[5] R. H. Friend, R. W. Gymer, A. B. Holmes, J. H. Burroughes, R. N. Marks, C. Taliani, D. D. C. Bradley, D. A. Dos Santos, J. L. Brédas, M. Lögdlund, and W. R. Salaneck, *Nature* **397**, 121 (1999).
[6] T. Matsumoto, T. Nakada, J. Endo, K. Mori, N. Kavamura, A. Yokoi, and J. Kido, *SID Int. Symp. Digest Tech. Papers*, **34**, 979 (2003).
[7] C. W. Chen, Y. J. Lu, C. C. Wu, E. H. E. Wu, C. W. Chu, and Y. Yang, *Appl. Phys. Lett.* **87**, 241121 (2005).
[8] L. S. Liao, K. P. Klubek, and C. W. Tang, *Appl. Phys. Lett.* **84**, 167 (2004).
[9] J. Drechsel, M. Pfeiffer, X. Zhou, A. Nollau, and K. Leo, *Synth. Met.* **127**, 201 (2002).
[10] X. D. Gao, J. Zhou, Z. T. Xie, B. F. Ding, Y. C. Qian, X. M. Ding, and X. Y. Hou, *Appl. Phys. Lett.* **93**, 083304 (2008).
[11] C. C. Chang, S. W. Hwang, C. H. Chen, and J. F. Chen, *Jpn. J. Appl. Phys. Part 1* **43**, 6418 (2004).
[12] C. C. Chang, J. F. Chen, S. W. Hwang, and C. H. Chen, *Appl. Phys. Lett.* **87**, 253501 (2005).
[13] H. Kanno, R. J. Holmes, Y. Sun, S. K. Cohen, and S. R. Forrest, *Adv. Mater.* **18**, 339 (2006).
[14] H. Kanno, N. C. Giebink, Y. Sun, and S. R. Forrest, *Appl. Phys. Lett.* **89**, 023503 (2006).
[15] L. S. Liao, X. F. Ren, W. J. Begley, Y. S. Tyan, and C. A. Pellow, SID 08 DIGEST 2008, p. 818.
[13] J. Kido, T. Nakada, J. Endo, N. Kawamura, K. Mori, A. Yokoi, and T. Matsumoto, in Proceedings of the 11th International Workshop on Inorganic and Organic Electrolumi
[17] nescence and 2002 International Conference on the Science and Technology of Emissive Displays and Lighting (2002), p. 539.
[18] P. E. Burrows, S. R. Forrest, S. P. Sibley, and M. E. Thompson, *Appl. Phys. Lett.* **69**, 2959 (1995).
[19] T. Y. Cho, C. L. Lin, and C. C. Wu, *Appl. Phys. Lett.* **88**, 111106 (2006).
[20] T. Tsutsui and M. Terai, *Appl. Phys. Lett.* **84**, 440 (2004).
[21] C. W. Law, K. W. Lau, M. K. Fung, M. Y. Chan, F. L. Wong, C. S. Lee, and S. T. Lee, *Appl. Phys. Lett.* **89**, 133511 (2006).
[22] M. K. Fung, K. M. Lau, S. L. Lai, C. W. Law, M. Y. Chan, C. S. Lee, and S. T. Lee, *J. Appl. Phys.* **104**, 034509 (2008).
[23] M. Y. Chan, S. L. Lai, K. M. Lau, M. K. Fung, C. S. Lee, and S. T. Lee, *Adv. Funct. Mater.* **17**, 2509 (2007).
[24] S. L. Lai, M. Y. Chan, M. K. Fung, C. S. Lee, and S. T. Lee, *J. Appl. Phys.* **101**, 014509 (2007).
[25] C. Shen, A. Kahn, and I. G. Hill, in *Conjugated Polymer and Molecular Interfaces*, edited by A. Kahn, J.-J. Pireaux, W. R. Salaneck, and K. Seki (Dekker, New York, 2001), p. 351.
[26] A. J. Mäkinen, M. Uchida, and Z. H. Kafafi, *Appl. Phys. Lett.* **82**, 3889 (2003).
[27] S. Naka, H. Okada, H. Onnagawa, and T. Tsutsui, *Appl. Phys. Lett.* **76**, 197 (2000).
[28] S. L. Lai, M. K. Fung, S. N. Bao, S. W. Tong, M. Y. Chan, C. S. Lee, and S. T. Lee, *Chem. Phys. Lett.* **367**, 753 (2003).
[29] T. C. Wong, J. Kovac, C. S. Lee, L. S. Hung, and S. T. Lee, *Chem. Phys. Lett.* **334**, 61 (2001).
[30] J. Wang, H. Wang, X. Yan, H. Huang, and D. Yan, *Appl. Phys. Lett.* **87**, 093507 (2005).
[31] K. M. Lau, J. X. Tang, H. Y. Sun, C. S. Lee, S. T. Lee, and D. Yan, *Appl. Phys. Lett.* **88**, 173513 (2006).

[Parts of this work were presented in Proceedings of IMID 2009.]